REPORT DOCUMENTATION PAGE

Form Approved OMB NO. 0704-0188

1. REPORT DATE (DD-MM-YYYY)	2. REPORT TYPE	3. DATES COVERED (From - To)
	New Reprint	-

4. TITLE AND SUBTITLE

Two-Dimensionally Ordered Plasmonic and MagneticNanostructures on Transferable Electron TransparentSubstrates

5a. CONTRACT NUMBER
W911NF-13-1-0428

5b. GRANT NUMBER

5c. PROGRAM ELEMENT NUMBER
611102

6. AUTHORS

Abhinav Malasi, Jingxuan Ge, Connor Carr, Hernando Garcia, Gerd Duscher, Ramki Kalyanaraman

5d. PROJECT NUMBER

5e. TASK NUMBER

5f. WORK UNIT NUMBER

7. PERFORMING ORGANIZATION NAMES AND ADDRESSES

University of Tennessee at Knoxville
1534 White Avenue

Knoxville, TN 37996 -1529

8. PERFORMING ORGANIZATION REPORT NUMBER

9. SPONSORING/MONITORING AGENCY NAME(S) AND ADDRESS (ES)

U.S. Army Research Office
P.O. Box 12211
Research Triangle Park, NC 27709-2211

10. SPONSOR/MONITOR'S ACRONYM(S)
ARO

11. SPONSOR/MONITOR'S REPORT NUMBER(S)
63702-PH.5

12. DISTRIBUTION AVAILIBILITY STATEMENT

Approved for public release; distribution is unlimited.

13. SUPPLEMENTARY NOTES

The views, opinions and/or findings contained in this report are those of the author(s) and should not contrued as an official Department of the Army position, policy or decision, unless so designated by other documentation.

14. ABSTRACT

Discovery of new plasmonic behaviors from nanostructured materials can be greatly accelerated by the ability to prepare and characterize their near-field behaviors with high resolution in a rapid manner. Here, an efficient and cost-effective way is reported to make 2D periodic nanostructures on electron transparent substrates for rapid characterization by transmission electron microscopy. By combining nanosphere lithography with a substrate float-off technique, large areas of electron transparent periodic nanostructures

15. SUBJECT TERMS

carbon, EELS, nanoparticles, nanosphere lithography, plasmons

16. SECURITY CLASSIFICATION OF:			17. LIMITATION OF ABSTRACT	15. NUMBER OF PAGES	19a. NAME OF RESPONSIBLE PERSON
a. REPORT	b. ABSTRACT	c. THIS PAGE			Ramakrishnan (Ramki) Kalyanaraman
UU	UU	UU	UU		19b. TELEPHONE NUMBER: 865-974-5539

Report Title

Two-Dimensionally Ordered Plasmonic and MagneticNanostructures on Transferable Electron TransparentSubstrates

ABSTRACT

Discovery of new plasmonic behaviors from nanostructured materials can be greatly accelerated by the ability to prepare and characterize their near-field behaviors with high resolution in a rapid manner. Here, an efficient and cost-effective way is reported to make 2D periodic nanostructures on electron transparent substrates for rapid characterization by transmission electron microscopy. By combining nanosphere lithography with a substrate float-off technique, large areas of electron transparent periodic nanostructures can be achieved. For this study, the synthesis of plasmonic nanostructures of Ag, magnetic nanostructures of Co, and bimetallic nanostructures of Ag–Co are investigated. Characterization of the materials by a combination of transmission electron microscopy, far-field optical spectroscopy, and magnetization measurements revealed that this new approach can yield useful nanostructures on transparent, flexible, and transferable substrates with desirable plasmonic and/or magnetic properties.

REPORT DOCUMENTATION PAGE (SF298)
(Continuation Sheet)

Continuation for Block 13

ARO Report Number 63702.5-PH
Two-Dimensionally Ordered Plasmonic and Mag...

Block 13: Supplementary Note

Approved for public release; distribution is unlimited.

Particle
& Particle Systems Characterization

Postfach 10 11 61
69451 Weinheim
Germany
Courier services:
Boschstraße 12
69469 Weinheim
Germany
Tel.: (+49) 6201 606 235 / 432
Fax: (+49) 6201 606 500
E-mail: particle@wiley.com

WILEY-VCH

Dear Author,

Please correct your galley proofs carefully and return them no more than three days after the page proofs have been received.

If you have not used the PXE system before, please view the Tutorial before checking your proofs: http://wileypxe.aptaracorp.com/pxewileyvch/UserDocument/UserGuide/WileyPXE5_AuthorInstructions.pdf

Please note any queries that require your attention. These are indicated with red Qs in the pdf or highlighted as yellow queries in the "Edit" window.

Please pay particular close attention to the following, as no further corrections can be made once the article is published online:

- **Names** of all authors present and spelled correctly
- **Titles** of authors are correct (Prof. or Dr. only: please note, Prof. Dr. is not used in the journals)
- **Addresses of all authors** and **e-mail address of the corresponding author** are correct and up-to-date
- **Funding bodies** have been included and grant numbers are accurate
- The **Title** of the article is OK
- All **figures** are correctly included
- **Equations** are typeset correctly

Note that figure resolution in the PXE system is deliberately lower to reduce loading times. This will be optimized before the article is published online.

Please send any additional information, such as figures or other display items, to particle@wiley.com, and please also indicate this clearly in the PXE "Edit" window by inserting a comment using the query tool.

Reprints may be ordered by filling out the accompanying form.
Return the reprint order form by e-mail with the corrected proofs, to Wiley- VCH: particle@wiley.com

Please limit corrections to errors already in the text. Costs incurred for any further changes will be charged to the author, unless such changes have been agreed upon by the editor.

The editors reserve the right to publish your article without your corrections if the proofs do not arrive in time. Note that the author is liable for damages arising from incorrect statements, including misprints.

Particle & Particle Systems Characterization

Editorial Office:

Wiley-VCH Verlag, Boschstrasse 12
69469 Weinheim, Germany

Tel.: (+49) 6201 606 235 or 432
Fax: (+49) 6201 606 500

Email: particle@wiley.com

Reprint Order Form 2015

Short DOI: ppsc. _____

Please send me and bill me for

☐ no. of **Reprints** via ☐ airmail (+ 25 Euro) ☐ surface mail

Please send me and bill me for a

☐ **high-resolution PDF file** (330 Euro).

My e-mail address:

_____

Please note: It is not permitted to present the PDF file on the internet or on company homepages

Information regarding VAT

Please note that from German sales tax point of view, the charge for **Reprints, Issues or Posters** is considered as **"supply of goods"** and therefore, in general, such delivery is a subject to German sales tax. However, this regulation has no impact on customers located outside of the European Union. Deliveries to customers outside the Community are automatically tax-exempt. Deliveries within the Community to institutional customers outside of Germany are exempted from the German tax (VAT) only if the customer provides the supplier with his/her VAT number. The VAT number (value added tax identification number) is a tax registration number used in the countries of the European Union to identify corporate entities doing business there. It starts with a country code (e.g. FR for France, GB for Great Britain) and follows by numbers.

Mail reprints / posters to:

_____
_____
_____
_____
_____

Invoice address:

_____
_____
_____
_____
_____

VAT no.: _____
(Institutes / companies in EU countries only)

Purchase Order No.: _____

Credit Card Payment:

VISA, MasterCard, AMERICAN EXPRESS

Please use the Credit Card Token Generator located at the website below to create a token for secure payment. The token will be used instead of your credit card number.

Credit Card Token Generator:
https://www.wiley-vch.de/editorial_production/index.php

Please transfer your token number to the space below.

Credit Card Token Number

Cover Posters

Posters are available of all the published covers and frontispieces in two sizes

☐ DinA2 42 x 60 cm/ 17 x 24in (one copy: **39 Euro**)

☐ DinA1 60 x 84 cm/ 24 x 33in (one copy: **49 Euro**)

Postage for shipping posters overseas by airmail:
+ 25 Euro

Postage for shipping posters within Europe by surface mail:
+ 15 Euro

Price list for reprints (The prices include mailing and handling charges. All Wiley-VCH prices are exclusive of VAT)

No. of pages	Price (in Euro) for orders of 50 copies	100 copies	150 copies	200 copies	300 copies	500 copies
1-4	345	395	425	445	548	752
5-8	490	573	608	636	784	1077
9-12	640	739	786	824	1016	1396
13-16	780	900	958	1004	1237	1701
17-20	930	1070	1138	1196	1489	2022
for every additional 4 pages	147	169	175	188	231	315

★ **Special Offer** ★ If you order 200 or more reprints you will get a PDF file for half price.

Wiley-VCH Verlag GmbH & Co. KGaA; Location of the Company: Weinheim;
Chairman of the Supervisory Board: Stephen Michael Smith,
Trade Register: Mannheim, HRB 432833, General Partner: John Wiley & Sons GmbH,
Location: Weinheim, Trade Register Mannheim, HRB 432296,
Managing Directors: Dr. Jon Walmsley, Sabine Steinbach

WILEY-VCH

Full Paper

xxxx

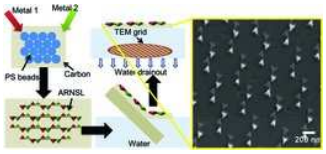

Synthesis of 2D periodic nanostructures on electron transparent carbon substrates is shown in this work. This is achieved by first depositing material through a mask of close-packed polystyrene spheres (nanosphere lithography), which produces nanostructures on an ultrathin carbon substrate. This is followed by a float-off technique that leads to electron transparent material.

ppsc201500048(201500048)

www.particle-journal.com

Particle & Particle Systems Characterization

Full Paper

Two-Dimensionally Ordered Plasmonic and Magnetic Nanostructures on Transferable Electron Transparent Substrates

By *Abhinav Malasi, Jingxuan Ge, Connor Carr, Hernando Garcia, Gerd Duscher, and Ramki Kalyanaraman**

Keywords: carbon, EELS, nanoparticles, nanosphere lithography, plasmons

ABSTRACT: Discovery of new plasmonic behaviors from nanostructured materials can be greatly accelerated by the ability to prepare and characterize their near-field behaviors with high resolution in a rapid manner. Here, an efficient and cost-effective way is reported to make 2D periodic nanostructures on electron transparent substrates for rapid characterization by transmission electron microscopy. By combining nanosphere lithography with a substrate float-off technique, large areas of electron transparent periodic nanostructures can be achieved. For this study, the synthesis of plasmonic nanostructures of Ag, magnetic nanostructures of Co, and bimetallic nanostructures of Ag–Co are investigated. Characterization of the materials by a combination of transmission electron microscopy, far-field optical spectroscopy, and magnetization measurements revealed that this new approach can yield useful nanostructures on transparent, flexible, and transferable substrates with desirable plasmonic and/or magnetic properties.

1. Introduction

The interaction of metallic and other conducting nanostructures with electromagnetic waves can result in important resonant interactions called surface or localized plasmons, which are being utilized in many different applications, including sensing, energy harvesting, data storage, catalysis, and more.[1–5] Progress in the field of plasmonics is primarily being driven by a good understanding of these resonant optical behaviors. In recent years there has been growing interest in correlating the near-field resonant behavior with the far-field optical properties as several differences, such as a red-shift in resonant position from near- to far- field has become evident.[6–16] Near-field studies have also revealed unique phenomenon such as hotspots due to strong electric fields, plasmon coupling effects such as hybridization, and fano resonances.[17–19] These near-field effects have been instrumental in enabling behaviors such as surface enhanced Raman sensing (SERS), localized plasmon resonance sensing, and Kerr rotation.[20–22] However, one of the important challenges in this field to discover better new materials that go beyond the traditional plasmonic materials of gold and silver.

One way to accelerate the discovery of better new plasmonic materials is by developing techniques to rapidly characterize the near-field behavior as a function of nanostrucure size, shape, spatial arrangement, composition, and environmental variables. However, these features can often vary rapidly within the length scale of a few nanometers or smaller. For example, the dipolar coupling between two closely spaced nanoparticles is strongly governed by the size of the gap.[23,24] Likewise, a small change in shape or composition can strongly influence the plasmonic signal.[25] Therefore, to keep pace with the explosion in the various nanomaterial synthesis techniques, we also need an accurate characterization of nanoscale plasmonic behavior by techniques that can probe and explore the nanomaterials at extremely high spatial as well as spectral energy resolution. Presently, the only known technique that can offer this ability is high resolution transmission electron microscopy (TEM). TEM has been central to the understanding of important properties of plasmonic materials, including the bulk plasmon energies, surface plasmon behaviors, magnetic circular dichroism, and ferroplasmons.[26–30] However, TEM has traditionally been a very time consuming technique due to

A. Malasi, Prof. R. Kalyanaraman, Department of Chemical and Biomolecular Engineering, University of Tennessee, Knoxville, TN 37996, USA
J. Ge, C. Carr, Prof. G. Duscher, Prof. R. Kalyanaraman, Department of Materials Science and Engineering, University of Tennessee, Knoxville, TN 37996, USA
Prof. H. Garcia, Department of Physics, Southern Illinois University, Edwardsville, IL 62026, USA
Q1 *Correspondence to*: Prof. R. Kalyanaraman (E-mail: ramki@vols.utk.edu)
10.1002/ppsc.201500048

the constraint placed by requiring electron transparent materials for the analysis.[31] This constraint often limits the number of samples one can investigate, thus restricting the pace of discovery of new plasmonic properties and materials.

Here we propose a way to accelerate nanostructure characterization enabled by localized probing and measurement of plasmonic behavior through a simple and time-efficient experimental approach to produce electron transparent nanostructures. Nanosphere lithography (NSL) has emerged as a good candidate for patterning large areas and is significantly cheaper than traditional lithography techniques such as e-beam or photoresist lithography.[32–35] Using this technique 2D periodic patterns can be obtained over large cm scale areas.[36–38] NSL involves the self-assembly of colloidal beads onto a substrate to yield a close-packed arrangement of spheres. This resulting system can then serve as a mask for the subsequent deposition of material using vapor deposition techniques.[39] This process leads to the synthesis of periodically arranged triangular structures, which then can be converted to semispherical shaped particles by thermal annealing.[32,40] A further modification of the NSL technique that expands its capabilities is by depositing the materials at an angle.[34,35,39,41] This angle resolved NSL (ARNSL), has been used to demonstrate the synthesis of nanostructures made from a combination of different materials, i.e., multicomponent nanostructures.[39] However, thus far, NSL has not been applied directly to make electron transparent substrates that can rapidly yield high quality nanostructures for TEM analysis.

Here we use NSL and ARNSL on ultrathin carbon substrates in combination with a water-based float-off (FO) process to yield large area ordered nanostructures directly as electron-transparent substrates. Specifically, we first demonstrate the synthesis and characterization of 2D periodic arrangements of a prototypical plasmonic metal, silver (Ag). Morphology studies by scanning electron microscopy (SEM) and TEM, as well as near- and far-field optical studies of the as-deposited and laser-heated Ag were used to determine the efficacy of this new technique. We also applied NSL + FO to prepare cobalt (Co) nanostructures and characterized their magnetic behavior using the surface magneto-optical Kerr rotation (SMOKE) technique. Finally, we combined ARNSL with FO to prepare bimetal nanostructures of the Co–Ag system and characterized them using SEM, TEM, and SMOKE. Collectively, these results demonstrated our goal of being able to easily make periodic nanostructure arrays on electron-transparent substrates. In addition, other advantages of this technique include the synthesis of large macroscopic areas of the 2D periodic structures on flexible and transferable substrates, thus also permitting several potentially useful applications of the nanostructure that are enabled by placing them on nonplanar shaped or flexible substrates.[36,42]

2. Method

The procedure yielding large area 2D periodic nanostructures on electron transparent carbon substrates involves three distinct steps (**Figure 1**). Step 1 is the creation of the NSL mask

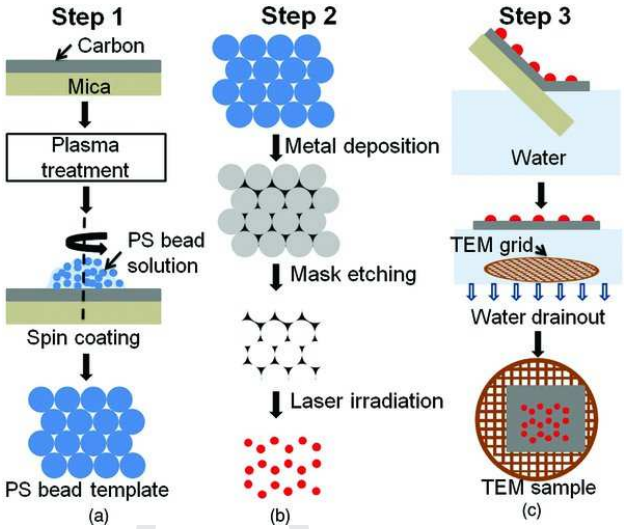

Figure 1. The schematic shows the three major steps for the TEM sample preparation. a) Step 1 of the synthesis, which is focused on NSL template formation. It shows the formation of NSL template on plasma treated carbon film on mica substrates. b) Step 2 is fabrication of nanostructures, which is achieved by depositing metal films and then etching out the template. Further heat treatment, such as with laser pulses, can be done to the metal nanostructures to change their shape. c) Step 3 is the float off of the carbon substrate with NSL structures on the water surface which is then captured on the TEM grid by draining the water.

and involves preparation of ultrathin carbon films on a rigid substrate followed by deposition of an array of close-packed polystyrene (PS) beads onto the substrate. The array of PS beads will serve as the deposition mask for the next step. Step 2 is the fabrication of nanostructures of the desired material and involves thin film deposition, etching of the PS spheres, and, if needed, a thermal processing step to transform the nanostructures. The final step, step 3, is the creation of the TEM sample and involves float-off to make the electron transparent material, which is captured directly onto a TEM grid for subsequent analysis. The specific details of the various steps involved are described in the following sections. Q2

2.1. Step 1: Creation of NSL Mask (Figure 1a) Q3

The initial substrate for use in the PS deposition was made by depositing carbon onto V-2 grade mica sheets purchased from Electron Microscopy Sciences Inc. Thin films of carbon were deposited on a freshly exposed surface of mica following removal of its top layers with the help of scotch tape. An amorphous carbon (a-C) of thickness in the range of 5 to 25 nm was sputter deposited using a SPI Inc. carbon coater under a vacuum of 10^{-4} Torr with a deposition rate of 5 nm min^{-1}.[43] After the deposition, the a-C films were treated in an oxygen plasma to make the top surface of carbon hydrophillic. The plasma treatment was done for 10 s using a Technics Inc. instrument operating at 8 V and a current of 10 mA. These plasma

treated carbon substrates could retain their hydrophilicity for almost 24 h. Following the plasma treatment, the carbon substrates were ready for the formation of a monolayer or bilayer of close packed PS beads. PS beads of size 500 nm in diameter were received as 2% w/v suspension in water from Alfa Aesar. NSL masks were then created by spin coating the solution of PS beads diluted with the mixture of Triton-X and methanol (1:400 volume ratio) in 1:1 volume ratio to achieve the hexagonal closed pack (HCP) arrangement of the beads.[32] The role of the surfactant, Triton-X, was to make the substrate wettable for the uniform spreading of the PS beads. To achieve the HCP arrangement, PS bead solution was spin coated at three different speeds using a programmable spin coater from Laurell Technologies Corporation model number WS-400BZ-8TFM/LITE. The three step coating consisted of spin coating at 400 rpm for 10 s to spread the PS beads uniformly, then at 800 rpm for 2 min to remove the excess material, and finally at 1400 rpm for 10 s to remove the bead accumulation occurring at the edges.[44] After this, the sample was left to dry under controlled environment (temperature maintained at 22 ± 1 with relative humidity at 40 ± 5%). Apart from the carbon substrate, the PS beads were also deposited onto glass, quartz and 400 nm SiO_2 coated Si substrates.

2.2. Step 2: Fabrication of Nanostructures (Figure 1b)

Once the mask was dried, the substrates were ready for the deposition of metal film onto them. Metal films of Ag and Co were deposited inside a vacuum chamber operating at a base pressure of 2×10^{-8} Torr to achieve monometal or bimetal systems. The Ag metal films were deposited using a Mantis QUAD-EV-HP e-beam evaporator while the Co films were deposited using Tectra e-beam evaporator. Metal targets of 99.999% purity from Alfa Aesar Inc. were used. Ag films in the thickness range of 5–40 nm were deposited, while Co films were deposited in the range of 2–10 nm. The deposition angle of the target metal could be controlled by rotating the sample holder. The deposition of the metals was done at 0° and ±10° with respect to the normal to the plane of substrate. Different samples of Co–Ag were made by depositing them at various angles mentioned. After the deposition of metal films, the PS mask was etched out by dipping the NSL substrates in dichloromethane. Depending on the thickness of the metal film, the etching time varied from few seconds to around 2 min. Once the PS beads were etched out, the carbon substrates with NSL or ARNSL were ready to be transferred on to the TEM grid. The deposited metal films on the carbon substrate were in the shape of triangles.[32,34] We also tested whether the shape could be changed by a thermal treatment of the nanostructures on the C/mica substrate. The Ag triangles made from 5 nm thick film were irradiated using nanosecond laser pulses to form semispherical nanoparticles. The Ag samples were irradiated using a 9 ns pulsed width Nd:YAG laser from Spectra Physics, which is an injection seeded Lab-130–50 laser operating at 266 nm wavelength with a repetition rate of 50 Hz. The Ag metal triangles were irradiated at normal incidence in ambient air environment using an energy density of 90 mJ cm^{-2} for 10 000 pulses with a beam size of 1 mm^2 .

2.3. Step 3: Creation of TEM Sample (Figure 1c)

The periodic arrays fabricated by NSL and ARNSL on carbon substrates were then floated off onto the surface of distilled water. Due to the hydrophobic nature of carbon and the weak forces of adhesion between the carbon and the mica surface, the surface tension of water was able to debond carbon from the mica surface resulting in an electron transparent C + nanostructure substrate. This substrate was directly captured onto a lacey carbon TEM grid by slowly draining of the water as detailed by Sachan et al.[43]

3. Characterization

The morphology of the NSL samples prepared on glass, quartz or 400 nm SiO_2 coated Si substrates were characterized using a Zeiss Merlin SEM operated at 1.7 kV. The synthesized NSL samples of Ag and Co were also characterized for their optical and magnetic properties. The far-field optical properties were studied in transmission mode using a HR2000 + ES spectrometer from Ocean Optics on glass and quartz substrates. The transmission spectrum was then converted to absorption spectrum using Beer–Lambert law. The magnetic study of the NSL samples was done using an in-house developed surface magneto-optical Kerr effect (SMOKE) system.[45,46] The SMOKE measurements were done in the longitudinal orientation using an s-polarized laser beam of 633 nm wavelength. The angle of incidence for the laser beam with the normal to the substrate plane was 12.6°. A Zeiss Libra 200 TEM was used to characterize the NSL samples on the carbon substrates by high angle annular dark field (HAADF) mode and electron energy-loss spectroscopy (EELS) at 200 kV. The TEM was equipped with a monochromator and omega shaped energy filter. The semiconvergent and semicollection angles were 9 and 11.9 mrad, respectively. The spatial and energy resolution of the monochromator equipped TEM in STEM mode was 0.3 nm and 0.15 eV, respectively. The low loss EELS was performed using a slit of 0.5 μm monochromator slit with an energy dispersion of 0.025 eV per channel for a exposure time of 0.1 s. Similarly, core loss EELS analysis was performed by using a 60 μm monochromator slit with an energy dispersion of 0.1 eV per channel for an exposure of 1 s. The incident electron beam current recorded for low loss and core loss EELS measurements was 1.577 and 131.58 pA, respectively. Bruker XFlash 5030 energy dispersive spectrometer (EDS) was used to gather the elemental information of the metals in the Zeiss Libra 200.

It is to be noted that the color contrast of the TEM and SEM images have been inverted for visual clarity. Since the imaging in the TEM was done in HAADF mode, so, the *Z*-contrast that is evident in HAADF imaging will be inverted, i.e., higher atomic number metals will appear darker in contrast in comparison to lower atomic number metals.

4. Results and Discussion

First, the application of NSL + FO leading to electron transparent nanostructures is presented for a prototypical plasmonic

metal, Ag. **Figure 2**a shows a SEM image of typical Ag nanotriangles formed by the NSL technique using normal incidence deposition of 5 nm thick Ag film onto quartz substrates. The inset of this image is a computer generated diffraction pattern from fast Fourier transform (FFT) analysis of the image contrast. The hexagonal symmetry was clearly evident. Figure 2b shows a magnified image to clearly show the repeating hexagonal unit for the Ag nanotriangles. Figure 2c shows the Ag nanoparticles formed after irradiating the Ag nanotriangles of Figure 2a using laser pulses. Figure 2d, which is a magnified image of (c), shows that each Ag triangle dewets into a collection of nanoparticles but retains the overall hexagonal symmetry. Figure 2e shows the TEM HAADF image of the nanotriangles formed on C substrate following the same NSL conditions as in Figure 2a. The overall pattern morphology and symmetry is similar to that observed in the SEM image (Figure 2a). An area of 15 × 15 μm^2 is covered by an array of nanotriangles arranged in hexagonal symmetry, as confirmed by the FFT shown in the inset of Figure 2e. This FFT was taken from the marked location of the image. Figure 2f, which is a magnified HAADF image of (e), was used to calculate the spacing and triangle size. The length of the angle bisector of the largest equilateral triangle than can fit was 115 nm while the spacing between the adjacent triangles was 290 nm. These values were consistent with the size and spacing expected for close packed arrangement of 500 nm sized beads.[32] Figure 2g shows the TEM HAADF image of Ag particles formed from the triangles after pulsed laser irradiation of the nanotriangles on C/mica substrate. While there is no change in the hexagonal arrangement of the triangles, as evidenced by the inset FFT, each nanotriangle transformed into a collection of 3 to 6 semispherical Ag nanoparticles, similar to that seen by the SEM in Figure 2d. From these results it was clear that NSL + FO can lead to nanostuctures similar to conventional NSL on rigid substrates and that the patterns could be thermally treated on the C substrates in order to further transform them.

Another motivation for this work was to show that high-quality electron transparent materials can be readily obtained and so we performed a low loss EELS study to characterize the plasmonic behavior of the Ag nanotriangles. **Figure 3** shows the low loss EELS study of a single Ag nanotriangle of thickness 10 nm deposited at 10° . Figure 3a shows the HAADF image of a single Ag nanotriangle of side lengths 110, 135, and 145 nm, while Figure 3b–d shows the EELS map of plasmon excitations at different energies: 1.35 ± 0.2, 2.5 ± 0.2, and 3.2 ± 0.2 eV, respectively, excited by the electron beam. The lightest (yellow) region represents the maximum plasmon scattering intensity while the dark (blue) regions represent the minimum scattering. This low loss EELS mapping of the Ag triangle on carbon substrate confirmed that the NSL + FO Ag samples also show various excitable plasmon modes on the Ag nanotriangles, as confirmed by previous TEM studies.[29]

Besides the potential applications that utilize the near-field properties of plasmons, such as in plasmon resonance sensing, the far-field optical and/or magnetic behavior of nanostructures are also important. In addition, in the future, this ability to fabricate large area ordered arrays on which both near-field TEM and far-field studies can be done simultaneously or sequentially (but on the same regions of the sample), to yield correlated

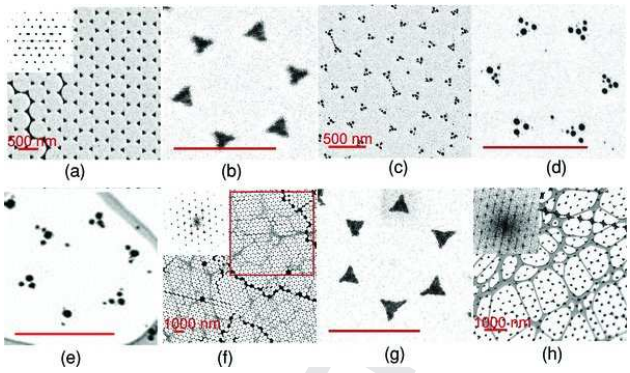

Figure 2. a) SEM images of Ag nanotriangles formed by NSL on quartz substrate. Inset shows the FFT of the contrast in (a) providing clear evidence for the hexagonal symmetry. b) Magnified image of the repeating Ag nanotriangle hexagonal pattern. c) SEM image of Ag nanoparticles formed by irradiation of Ag nanotriangles on quartz using pulsed laser heating. d) Magnified image of the irradiated Ag nanotriangles. e) TEM HAADF image of the Ag nanotriangles formed by NSL + FO. The underlying lacey carbon film of the TEM substrate is also evident. Inset shows the FFT (taken from the red square) showing evidence for the hexagonal symmetry of the spatial arrangement. f) Magnified TEM image of the Ag nanotriangle repeating unit. g) TEM HAADF image of the Ag nanoparticles transformed from nanotriangles following irradiation by laser pulses formed by NSL + FO. Inset FFT shows the hexagonal symmetry. h) The magnified image of the irradiated Ag nanotriangle patterns. The scale bar on the individual hexagonal ring images is 500 nm.

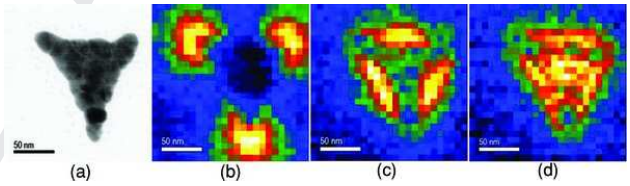

Figure 3. Low loss EELS mapping of a Ag nanotriangle on C substrate. a) HAADF image of Ag nanotriangle. b–d) Map of different plasmon modes excited by the e-beam b) corresponds to an energy of 1.35 eV, c) is for 2.5 eV, and d) is 3.2 eV.

properties from complementary techniques could be tremendously powerful in our quest for new nanomaterials. Here, we performed far-field studies of the optical and magnetic properties of the various triangles made on quartz substrates. In **Figure 4**a the far-field optical absorbance measured for light incident normal to the substrate plane is compared for Ag nanotriangles formed from different film thickness. As the film thickness increased, the strong absorption peak corresponding to a localized surface plasmon resonance (LSPR) was found to blue-shift, consistent with the earlier studies of Jensen et al.[33] and Chan et al.,[47] who attributed it to a pyramidal-shape effect. The far-field LSPR behavior for Ag semispherical nanoparticles formed by laser irradiation of 5 nm thick Ag nanotriangles (whose LSPR is not shown here since it is at a wavelength be-

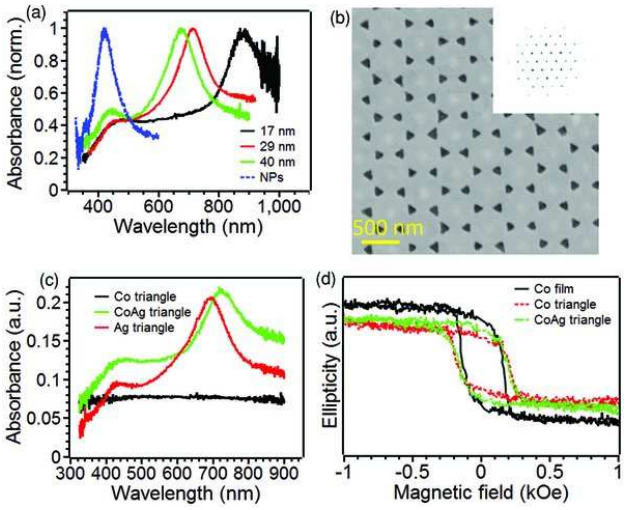

Figure 4. a) Far-field optical absorption spectrum of Ag nanotriangles for various thickness of the triangular nanostructures. Also shown is the absorption spectrum for the Ag nanoparticles formed by pulsed laser heating (dashed blue line). b) SEM morphology of Co nanotriangles from NSL on quartz, with inset showing the FFT hexagonal pattern. c) Comprison of the far field optical absorption spectrum from Co, Ag, and Co–Ag nanotriangles deposited at 10°, respectively. d) Magnetic hysteresis measured by SMOKE technique in longitudinal geometry comparing a Co film (solid black line), NSL Co nanotriangles (dotted red line), and NSL Co–Ag triangles (dashed green line).The Co triangles were deposited at 10° and Co–Ag was deposited at 10° and −10°, respectively.

yond 1000 nm) is shown by the dashed blue line. The LSPR of the Ag nanoparticles is substantially blue shifted as compared to the nanotriangles it was made from, which is consistent with the shape effect discussed previously.[33] Figure 4b shows the SEM morphology of Co nanotriangles formed by NSL by deposition of 10 nm thick film at 10°. The inset again depicts the hexagonal symmetry. Figure 4c compares the optical absorption spectrum of Co (10 nm) and Ag (29 nm) samples deposited at 10°. Unlike Ag, pure Co does not show a strong plasmonic signal in the visible wavelength (Figure 4c, black line), consistent with our recent results on Ag and Co nanoparticles.[26] However, since Co is ferromagnetic, it shows strong magneto-optical character, which can be used to measure its magnetic hysteresis. This measurement is shown in Figure 4d, which compares the hysteresis of a continuous Co film (solid black line) with the NSL Co nanotriangles (dotted red line).

Given the growing number of plasmonic discoveries related to the use of multicomponent materials and interest in applications pertaining to strong magneto-optical behavior from bimetallic materials,[19,26,48–53] we investigated the possibility to control the synthesis of bimetal nanostructures on quartz and the electron transparent C substrates using the NSL technique. As has been described by Nemiroski et al.,[39] ARNSL can yield a variety of geometries of nanostructures made from multiple different materials. Here, we extended this technique to directly making electron transparent substrates, something not demonstrated earlier. We compared the ARNSL model prediction for simple Co–Ag nanotriangle structures and characterized them using TEM and SMOKE techniques, as discussed next.

The capability of making various nanostructures using ARNSL is achieved by using the projection of shadows casted by beads in the path of the material flux being deposited. Mathematically, the shadows can be modeled by simply taking the projection of the bead when obstructed by a light source, which is elliptical in shape. With respect to **Figure 5**a, The elliptical shadow of the PS bead can be described as $y = \frac{R\mathrm{Sin}\theta \pm \sqrt{R^2 - x^2}}{\mathrm{Cos}\theta}$, where R is the radius of PS bead and θ is the projection angle of material being deposited.[54] The pattern formation for ARNSL depends on the orientation of the HCP structures formed by PS beads with respect to the line of sight of deposition.[54] The difference in the patterns depend on the two different angles as shown in the schematic in Figure 5a. The angle Φ tells the orientation of the HCP structure with respect to the fixed axis in the x–y plane and θ is the angle made by the material deposition vector ($\vec{p}$) with the z-axis. By controlling these angles a wide variety of structures can be formed as can be seen in Figure 5. Some of these structures have been simulated to show how the variation in the structures can be made using ARNSL. Figure 5b shows a single metal deposited at $\theta = 0°$ and $\Phi = 0°$. Figure 5c,d shows the theoretical structure for deposition of bimetals (shown by red and blue color) at $\theta = \pm 10°$ and $\Phi = 0°$ and 90°, respectively. In Figure 5e,f, the experimental SEM image for bimetal Ag and Co deposition under the conditions of (c) is shown, with (f) being the magnified image of a repeating hexagonal unit. The difference in contrast for the two metals is due to their different atomic (Z) numbers. The comparison shows that each hexagonal ring is made of pairs of metal triangles arranged in a similar fashion for the simulated and experimental cases. Similarly, Figure 5g,h corresponds to the experimental structure for Ag and Co generated with the conditions for the image shown in (d). Figure 5h is a magnified image showing the repeat unit for the SEM image shown in (g). Similarity in arrangement of the pairs of triangles with the theoretical prediction is evident.

Next, the synthesis of bimetal Co–Ag triangles on the electron transparent substrates was also tested. **Figure 6**a shows the TEM HAADF image of the overlapping triangles formed by deposition of the individual metals onto C at 10° and −10°, respectively, with respect to the normal to the substrate plane. The deposited films of Ag and Co were 10 nm each in thickness. The color contrast in the HAADF images comes from the difference in the Z-number of the two elements (inverted as mentioned earlier under Section 3). The darker triangles correspond to Ag and the lighter ones to Co. In Figure 6b, a magnified HAADF image of one pair of triangles (marked by the red circle in Figure 6a) is shown. This triangle pair was mapped for its elemental distribution using core loss EELS. Figure 6c,d shows the core loss EELS elemental mapping of Ag and Co metal, respectively. Figure 6c was generated using the Ag-M4,5 ionization edge at 367 eV. The map also represented the thickness profile of Ag using core loss EELS analysis. Similarly, the thickness profile of the Co region is shown in Figure 6d, and was generated using the Co-L2,3 ionization edge at 779

Particle & Particle Systems Characterization www.particle-journal.com

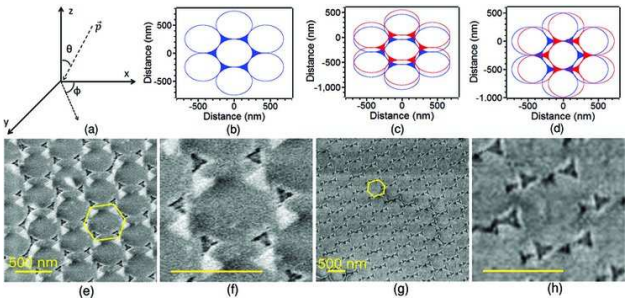

Figure 5. a) The coordinate system for the modeling of ARNSL. x–y is the plane of the substrate with z-axis acting as the normal to the plane. $\vec{p}$ is the vector denoting the direction of the metal flux and makes an angle θ with the z-axis. Φ is the orientation of the HCP with respect to the coordinate system. Some of the simulated patterns are shown in: b) Simulated pattern for a single metal deposition with $\theta = 0^\circ$ and $\Phi = 0^\circ$. c) Simulated pattern of bimetals deposited at $\theta = \pm 10^\circ$, $\Phi = 0^\circ$. d) Simulated pattern for $\theta = \pm 10^\circ$, $\Phi = 90^\circ$. e) Experimental SEM image of Ag (bright triangles) and Co (dark triangles) deposited for the conditions in (c). f) SEM image of repeating hexagonal pattern shown in (e). g) Experimental SEM image of Ag (bright triangles) and Co (dark triangles) deposited for the conditions in (d). h) SEM image of the repeating unit shown in (g). A hexagon is marked in the SEM images for reference and to show the repeating units of NSL. The length of the scale bars in (f) and (h) are of 500 nm each.

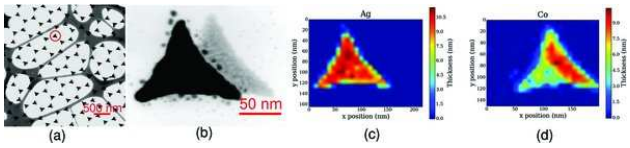

Figure 6. a) The HAADF image of Co–Ag nanotriangles formed by deposition at 10° and −10°, respectively. b) A magnified HAADF image of one pair of Co–Ag nanotriangles, encircled in (a). c) Core loss EELS map yielding the thickness of Ag in the structure shown in (b). Core loss EELS map yielding the thickness of Co for the structure shown in (b).

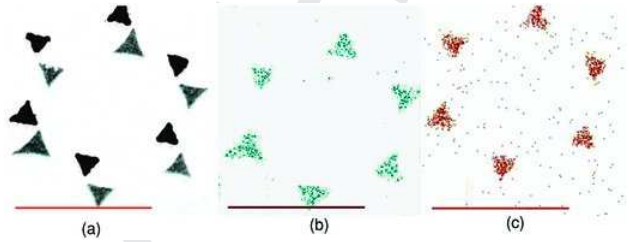

Figure 7. Elemental mapping of Ag and Co using EDS in the TEM. a) HAADF image of Co (dark) and Ag (bright) triangles. b) EDS map of Co across the HAADF image shown in (a). c) EDS map of Ag across the HAADF image shown in (a). The scale bar is of 500 nm length.

eV. The optical and magnetic behavior of this Co–Ag is shown in Figure 4c,d, respectively. The overlap of the Co with Ag shifts the Ag LSPR to red wavelengths, an effect previously reported for bimetallic nanoparticles of Ag–Co.[55] The hysteresis measured by SMOKE, and shown in Figure 4(d, dashed green line) confirmed the ferromagnetic character of the Co triangles in contact with Ag. It should be noted that our SMOKE measurements were made with a 633 nm laser, far from the LSPR peak location of ≈750 nm seen for this bimetal triangle system in Figure 4c. Therefore, the enhanced magneto-optical signal that is expected around the LSPR resonance was not detected in our measurements.[56] A different set of Co–Ag triangles on the electron transparent carbon substrate was also investigated by elemental mapping using the EDS technique in the TEM. The hexagonal arrangement of the triangle can be seen in the HAADF image shown in **Figure 7**a. The Co and Ag were deposited at 10° and −10°, respectively. Figure 7b,c shows the EDS maps of Co (blue) and Ag (red) metals, respectively. From these results we concluded that predictable electron transparent samples containing multiple different materials can be prepared by the NSL + FO technique.

5. Conclusion

We have described a simple and efficient way to make 2D periodic nanostructures of different metals on electron transparent substrates. Nanostructures of plasmonic Ag, ferromagnetic Co, and bimetal structures of Co–Ag were synthesized by nanosphere lithography on ultrathin carbon films. The nanostructure array/carbon system could be easily detached from an underlying mica support by immersion in water, resulting in transferable, flexible, and large area electron transparent materials. This technique could help accelerate discovery of new plasmonic phenomenon and/or better nanostructured materials for plasmonic and magnetic applications.

Acknowledgements

The authors acknowledge support by the Army Research Office through Grant No. W911NF-13–1–0428. A portion of this research was conducted under Grant No. CNMS2013–284 at the Center for Nanophase Materials Science, which is sponsored at ORNL by the Scientific User Facilities Division, Office of Basic Energy Sciences, U.S. Department of Energy. The authors would also like to acknowledge the use of TEM facilities housed by Joint Institute of Advanced Materials (JIAM) at University of Tennessee Knoxville.

Received: April 9, 2015
Revised: June 23, 2015
Published Online: MM DD, YYYY

[1] O. Primera-Pedrozo, J. I. Jerez-Rozo, E. Cruz-Montoya, T. Luna-Pineda, L. C. Pacheco-Londono, S. Hernández-Rivera, *IEEE Sens. J.* **2008**, *8*, 963.

[2] A. V. Kabashin, P. Evans, S. Pastkovsky, W. Hendren, G. A. Wurtz, R. Atkinson, R. Pollard, V. A. Podolskiy, A. V. Zayats, *Nat. Mater.* **2009**, *8*, 867.
[3] H. A. Atwater, A. Polman, *Nat. Mater.* **2010**, *9*, 205.
[4] D. O'Connor, A. V. Zayats, *Nat. Nanotechnol.* **2010**, *5*, 482.
[5] S. Linic, P. Christopher, D. Ingram, *Nat. Mater.* **2011**, *10*, 911.
[6] B. Gallinet, O. J. F. Martin, *Opt. Express* **2011**, *19*, 22167.
[7] P. A. Gonzalez, P. Albella, F. Neubrech, C. Huck, J. Chen, F. Golmar, F. Casanova, L. E. Hueso, A. Pucci, J. Aizpurua, R. Hillenbrand, *Phys. Rev. Lett.* **2013**, *110*, 203902.
[8] M. D. Doherty, A. Murphy, R. J. Pollard, P. Dawson, *Phys. Rev. X* **2013**, *3*, 011001.
[9] J. Zuloaga, P. Nordlander, *Nano Lett.* **2011**, *11*, 1280.
[10] B. Grzeskiewicz, K. Ptaszynski, M. Kotkowiak, *Plasmonics* **2014**, *9*, 607.
[11] C. Menzel, E. Hebestreit, S. Muhlig, C. Rockstuhl, S. Burger, F. Lederer, T. Pertsch, *Opt. Express* **2014**, *22*, 9971.
[12] F. Moreno, P. Albella, M. Nieto-Vesperinas, *Langmuir* **2013**, *29*, 6715.
[13] M. Rahmani, E. Yoxall, B. Hopkins, Y. Sonnefraud, Y. Kivshar, M. Hong, C. Phillips, S. A. Maier, A. E. Miroshnichenko, *ACS Nano* **2013**, *7*, 11138.
[14] J. M. Sanz, D. Ortiz, R. Alcaraz de la Osa, J. M. Saiz, F. Gonzalez, A. S. Brown, M. Losurdo, H. O. Everitt, F. Moreno, *J. Phys. Chem. C* **2013**, *117*, 19606.
[15] A. Yanai, M. Grajower, G. M. Lerman, M. Hentschel, H. Giessen, U. Levy, *ACS Nano* **2014**, *8*, 4969.
[16] B. M. Ross, S. Tasoglu, L. P. Lee, *Plasmonics: Metallic Nanostructures and Their Optical Properties VII*, **2009**.
[17] H. Wang, D. W. Brandl, F. Le, P. Nordlander, N. J. Halas, *Nano Lett.* **2006**, *6*, 827.
[18] E. Prodan, C. Radloff, N. J. Halas, P. Nordlander, *Science* **2003**, *302*, 419.
[19] G. Bachelier, I. Russier-Antoine, E. Benichou, C. Jonin, N. Del Fatti, F. Vallee, P. F. Brevet, *Phys. Rev. Lett.* **2008**, *101*, 197401.
[20] Y. Sun, Y. Xia, *Anal. Chem.* **2002**, *74*, 5297.
[21] S. Tripathy, R. Marty, V. K. Lin, S. L. Teo, E. Ye, A. Arbouet, L. Saviot, C. Girard, M. Y. Han, A. Mlayah, *Nano Lett.* **2011**, *11*, 431.
[22] P. K. Jain, Y. Xiao, R. Walsworth, A. E. Cohen, *Nano Lett.* **2009**, *9*, 1644.
[23] T. Atay, J. H. Song, A. V. Nurmikko, *Nano Lett.* **2004**, *4*, 1627.
[24] A. N. Grigorenko, A. K. Geim, H. F. Gleeson, Y. Zhang, A. A. Firsov, I. Y. Khrushchev, J. Petrovic, *Nature* **2005**, *438*, 335.
[25] S. Link, M. A. El-Sayed, *J. Phys. Chem. B* **1999**, *103*, 8410.
[26] R. Sachan, A. Malasi, J. Ge, S. Yadavali, H. Krishna, A. Gangopadhyay, H. Garcia, G. Duscher, R. Kalyanaraman, *ACS Nano* **2014**, *8*, 9790.
[27] W. Zhou, S. J. Pennycook, J. C. Idrobo, *Ultramicroscopy* **2012**, *119*, 51.
[28] P. Schattschneider, S. Rubino, C. Hebert, J. Rusz, J. Kunes, P. Novak, E. Carlino, M. Fabrizioli, G. Panaccione, G. Rossi, *Nat. Lett.* **2006**, *441*, 486.
[29] J. Nelayah, M. Kociak, O. Stephan, F. J. Garcia de Abajo, M. Tence, L. Henrard, D. Taverna, I. Pastoriza-Santos, L. M. Liz-Marzan, C. Colliex, *Nat. Phys.* **2007**, *3*, 348.
[30] R. F. Egerton, *Rep. Prog. Phys.* **2009**, *72*, 016502.
[31] S. Rao, K. Muraleedharan, C. Humphreys, *Microscopy: Science, Technology, Applications and Education*, Formatex Research Center, **2010**.
[32] J. C. Hulteen, R. P. Van Duyne, *J. Vac. Sci. Technol. A* **1995**, *13*, 1553.
[33] T. R. Jensen, M. D. Malinsky, C. L. Haynes, R. P. Van Duyne, *J. Phys. Chem. B* **2000**, *104*, 10549.
[34] C. L. Haynes, A. D. McFarland, M. T. Smith, J. C. Hulteen, R. P. Van Duyne, *J. Phys. Chem. B* **2002**, *106*, 1898.
[35] C. L. Haynes, R. P. Van Duyne, *Nano Lett.* **2003**, *3*, 939.
[36] N. Vogel, S. Goerres, K. Landfester, C. K. Weiss, *Macromol. Chem. Phys.* **2011**, *212*, 1719.
[37] S. M. Weekes, F. Y. Ogrin, W. A. Murray, P. S. Keatley, *Langmuir* **2007**, *23*, 1057.
[38] X. Meng, D. Qiu, *Langmuir* **2014**, *30*, 3019.
[39] A. Nemiroski, M. Gonidec, J. M. Fox, P. Jean-Remy, E. Turnage, G. M. Whitesides, *ACS Nano* **2014**, *8*, 11061.
[40] C. M. Muller, F. C. F. Mornaghini, R. Spolenak, *Nanotechnology* **2008**, *19*, 485306.
[41] A. V. Whitney, B. D. Myers, R. P. Van Duyne, *Nano Lett.* **2004**, *4*, 1507.
[42] C. W. Kuo, J. Y. Shiu, Y. H. Cho, P. Chen, *Adv. Mater.* **2003**, *15*, 1065.
[43] R. Sachan, A. Malasi, S. Yadavali, B. Griffey, J. Dunlap, G. Duscher, R. Kalyanaraman, *Part. Part. Syst. Charact.* **2015**, *32*, 476.
[44] C. L. Cheung, R. J. Nikoli, C. E. Reinhardt, T. F. Wang, *Nanotechnology* **2006**, *17*, 1339.
[45] N. Shirato, H. Krishna, A. K. Gangopadhyay, R. Kalyanaraman, *Instrumentation, Metrology, Standards for Nanomanufacturing IV*, **2010**.
[46] N. Shirato, *Ph.D. Thesis*, University of Tennessee Knoxville, **2012**.
[47] G. H. Chan, J. Zhao, E. M. Hicks, G. C. Schatz, R. P. Van Duyne, *Nano Lett.* **2007**, *7*, 1947.
[48] V. V. Temnov, G. Armelles, U. Woggon, D. Guzatov, A. Cebollada, A. Garcia-Martin, J. M. Garcia-Martin, T. Thomay, A. Leitenstorfer, R. Bratschitsch, *Nat. Photonics* **2010**, *4*, 107.
[49] T. Shegai, S. Chen, V. D. Miljkovic, G. Zengin, P. Johansson, M. Kall, *Nat. Commun.* **2011**, *2*, 481.
[50] N. Liu, M. L. Tang, M. Hentschel, H. Giessen, A. P. Alivisatos, *Nat. Mater.* **2011**, *10*, 631.
[51] D. Rudolf, C. La-O-Vorakiat, M. Battiato, R. Adam, J. M. Shaw, E. Turgut, P. Maldonado, S. Mathias, P. Grychtol, H. T. Nembach, T. J. Silva, M. Aeschlimann, H. C. Kapteyn, M. M. Murnane, C. M. Schneider, P. M. Oppeneer, *Nat. Commun.* **2012**, *3*, 1037.
[52] V. I. Belotelov, L. E. Kreilkamp, I. A. Akimov, A. N. Kalish, D. A. Bykov, S. Kasture, V. J. Yallapragada, A. V. Gopal, S. I. Grishin, A. M. Khartsev, M. Nur-E-Alam, M. Vasiliev, L. L. Doskolovich, D. R. Yakovlev, K. Alameh, A. K. Zvezdin, M. Bayer, *Nat. Commun.* **2013**, *4*, 2128.
[53] A. Holewinski, J. C. Idrobo, S. Linic, *Nat. Chem.* **2014**, *6*, 828.
[54] A. Kosiorek, W. Kandulski, P. Chudzinski, K. Kempa, M. Giersig, *Nano Lett.* **2004**, *4*, 1359.
[55] R. Sachan, S. Yadavali, N. Shirato, H. Krishna, V. Ramos, G. Duscher, S. J. Pennycook, A. K. Gangopadhyay, H. Garcia, R. Kalyanaraman, *Nanotechnology* **2012**, *23*, 275604.
[56] J. B. Gonzalez-Diaz, A. Garcia-Martin, J. M. Garcia-Martin, A. Cebollada, G. Armelles, B. Sepulveda, Y. Alaverdyan, M. Kall, *Small* **2008**, *4*, 202.

Q1 APT to AU: Please provide the highest academic title (either Dr. or Prof.) for all authors, where applicable.
Q2 APT to AU: Please check edits to the preceding text are OK and that the meaning has not been changed.
Q3 APT to AU: Please check the edits done in the subsections of Section 3.
Q4 APT to AU: Please add publisher name and location in refs. 16 and 45.
Q5 APT to AU: Please add publisher location in ref. 31.